pH-Controlled Nanoaggregation in Amphiphilic Polymer Co-networks

Gabriel S. Longo,[†] Monica Olvera de la Cruz,[†,*] and Igal Szleifer[‡,*]

[†]Department of Materials Science and Engineering and [‡]Department of Biomedical Engineering and Department of Chemistry, Northwestern University, 2170 Campus Drive, Evanston, Illinois 60208, United States

ABSTRACT Domain formation and control in pH-responsive amphiphilic polymer co-networks are studied theoretically. Two different molecular architectures of the polymer network are considered, depending on whether the pH-sensitive motif is borne by the hydrophobic or the hydrophilic monomer. When the hydrophobic polymer contains acidic groups, such chains form nanometric aggregates at acidic conditions, but they are found in a swollen state at alkaline pH. At intermediate pH, the nanoaggregation behavior of the hydrophobic polymer depends critically on the environment salt concentration. Moreover, our results indicate the presence of microphase separation into domains of swollen and aggregated hydrophobic chains. If the hydrophilic polymer is the ionizable component of the network, the nanoaggregation of hydrophobic monomers is weakly dependent on the pH and salt concentration, and except at very low volume fraction, the aggregate is the most probable conformation of the network in the entire range of pH and salt concentration studied. The two different hydrogels display quantitatively similar swelling transition and apparent pK_a, but at the nanoscale, their behavior is qualitatively different. The spatial distribution of electric charge on the network as well as the local density of the different chemical species within the hydrogel can be controlled, as a function of pH and salt concentration, by the molecular architecture of the polymer network. These findings have relevance for applications in biomaterials and nanotechnology, in particular, in the design of oral delivery devices for the administration of hydrophobic drugs.

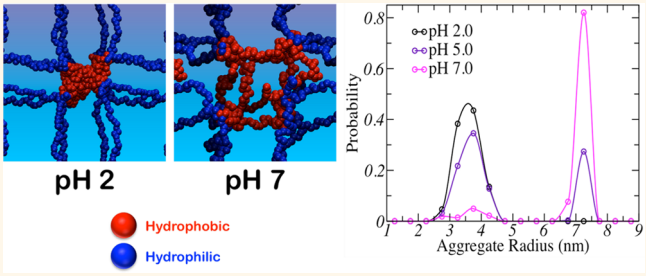

KEYWORDS: hydrogels · amphiphilic copolymer networks · responsive materials · nanoaggregation · drug delivery

Stimuli-responsive hydrogels are cross-linked polymer networks that can perform mechanical work in response to modifications in their environment. The stimuli include external changes of the physical properties of the system such as its temperature,[1,2] electric field,[3−6] and exposure to light,[7] but also changes in the chemical composition of the solvent such as its quality,[8,9] pH,[10−12] ionic strength,[11] and concentration of biomolecules.[13] The environment-controlled behavior of these polymer hydrogels is well-suited for the development of a variety of applications that include, but are not limited to, superadsorbent materials,[14] electrolyte batteries,[15] microfluidic devices,[16] microactuators,[17] and artificial muscles.[5,18−20] Moreover, in biomedical and biomaterials research,[21] the use of responsive hydrogels has found novel applications in drug delivery,[22−24] tissue engineering,[25] biosensors,[26] and intelligent materials that can imitate biological functions.[27]

Due to the large changes in pH that occur along the digestive track, pH-sensitive hydrogels are generally used in drug delivery to achieve controlled oral administration.[22,23,28−31] These hydrogels can swell many times their volume in response to changes in the pH of the environment as a result of the presence of acidic (or basic) groups on the polymer network.[23] Since the release of the molecule generally occurs by diffusion in the swollen polymer network, which has an intrinsically high water affinity, pH-sensitive gels have been mainly considered for the delivery of hydrophilic drugs.[32] However, an increasing number of anticancer drugs and many proteins are hydrophobic, which constrains the use of a swellable hydrophilic polymer network for the oral administration of such molecules. In this work, we use a molecular-level theory to study the structure and thermodynamic behavior of amphiphilic polymer co-networks. In particular, we concentrate our attention on how nanostructures within the gel can

* Address correspondence to m-olvera@northwestern.edu; igalsz@northwestern.edu.

Received for review January 9, 2013 and accepted February 25, 2013.

Published online February 25, 2013
10.1021/nn400130c

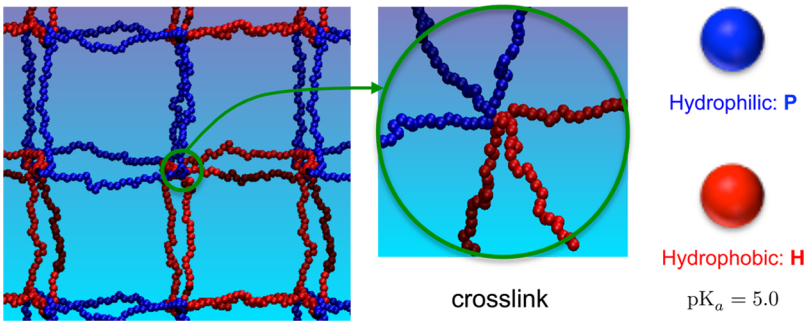

Figure 1. Schematic representation of the highly swollen amphiphilic polymer co-network. The polymer volume fraction is ϕ_G = 0.003. Each nodal monomer is cross-linking three hydrophobic and three hydrophilic polymer chains; there are 25 monomers in each chain; the polymer segment length is 0.5 nm.

be controlled by solution variables, such as pH and solution ionic strength, for different molecular architectures of the gel. Moreover, we study how modifying bulk properties changes the nanostructure and local environments, *e.g.*, local pH and ion concentration.

Molecular design of the hydrogel can provide the answer to achieve efficient loading and release of hydrophobic drugs through the modification of the hydrogel nanostructure to incorporate hydrophobic motifs within the swellable template.[33] Amphiphilic polymer co-networks (APCNs) are hydrogels that contain both hydrophilic or polar (P) and hydrophobic (H) monomers.[34,35] APCNs are widely used as materials for soft contact lenses[35,36] and hold great potential for the development of surface coatings with nonfouling properties,[37] antimicrobial coatings,[38] drug delivery devices,[39] and scaffolds for tissue engineering.[40] Enzymatic activity in organic solvents can be enhanced by their encapsulation into a nanophase-separated amphiphilic network, as demonstrated by Bruns *et al.*[41] Moreover, responsive hydrophobic−hydrophilic block copolymer gels show promising features for the design of photonic materials with exceptional flexibility to tailor the device stop-band.[42] The use of these copolymer networks as membranes for the separation of water/ethanol mixtures *via* pervaporation has also been investigated.[43] In addition, amphiphilic copolymer networks have been considered for the development of responsive materials that can mimic pancreatic activity.[44,45]

One of the key features of polymer networks containing hydrophobic groups is that they may display microphase separation in water,[34,46,47] and depending on the molecular architecture of a pH-responsive amphiphilic co-network, nanophase separation can be observed.[48] The behavior of APCNs is determined by the competition between chemical equilibrium, molecular organization, and physical interactions: nanoaggregation in water is driven by hydrophobic attractions among the nonpolar segments, while the electrostatic repulsions between charged monomers oppose this aggregation. This balance is more subtle when the polymer segments are charge regulating, *i.e.*, acids or bases, whose state of protonation can be controlled with pH and salt concentration. We have recently considered the swelling of model poly(acrylic acid) gels[49] and shown that the pH within the gels is different from that of the bulk solution. Therefore, the degree of protonation of the acid groups is different from what would be expected from bulk pH considerations. This is due to the confinement of the acidic groups within the gel that, if charged, results in very large electrostatic repulsions. As a result, the acid−base equilibrium is shifted toward the protonated (uncharged) species to relax some of the repulsions. The shift is even more pronounced when the polymers are hydrophobic, as has been recently shown in a grafted polymer layer where domain formation was predicted.[50] How do these effects determine the nanodomain formation on APCNs?

We have considered two different molecular architectures of APCN depending on whether the ionizable component of the network is the hydrophobic or the hydrophilic polymer. Our findings show that the nanoaggregation of hydrophobic chains, when such polymer chains bear pendant acidic groups, can be controlled by the environment pH (bath pH). The pH-responsive behavior can be useful to engineer devices for the targeted delivery of hydrophobic drugs. For example, the drug can be accurately localized within the hydrogel in the hydrophobic pockets at the pH where they are aggregated. The hydrophobic drug's release can be externally controlled by varying the pH. In addition, the molecular design of the amphiphilic network provides a way to precisely control, as a function of the bath pH and salt concentration, the spatial distribution of charge on the network and the chemical composition within the hydrogel.

RESULTS

In this work we present theoretical predictions for APCNs with the molecular structure shown in Figure 1. The networks are composed of cross-linked block copolymers of equal length, where one monomer is hydrophobic (red) while the other is hydrophilic (blue).

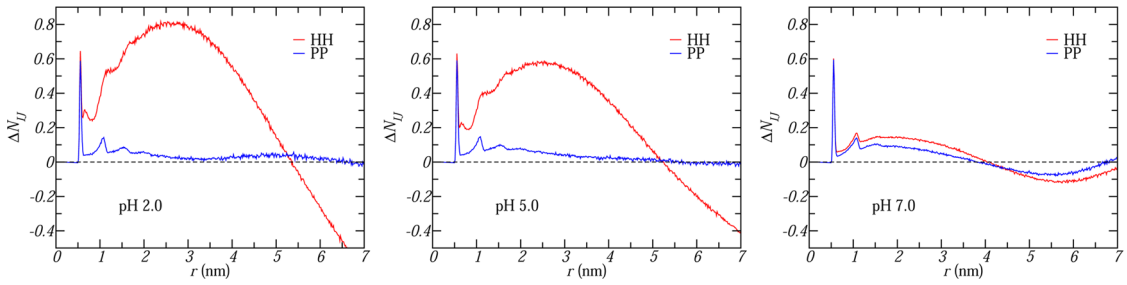

Figure 2. $\Delta N_{IJ}(r)$ between pairs of hydrophobic (HH) and hydrophilic (PP) monomers at different pH. The salt concentration is c = 100 mM, and the polymer volume fraction ϕ_G = 0.013. The dashed line shows the y-axis.

We are interested in pH-responsive networks; therefore, some of the monomers are functionalized with an acidic group. The only difference between the two networks we have considered is whether the functionalized monomer (acid) is hydrophobic (H) or hydrophilic (P). The type of monomers that can form the networks modeled in this work are poly(4-vinylbenzoic acid), which is not soluble in water at low pH,[51] and poly(acrylic acid), which is hydrophilic, as examples of the ionizable polymers. The hydrophobic poly(styrene) and the hydrophilic poly(ethylene oxide) are examples of the nonionizable polymers. A H(i)-P(n) APCN, which has ionizable hydrophobic and nonionizable hydrophilic monomers, is described in the next section, followed by a comparison with H(n)-P(i) APCN, *i.e.*, with nonionizable hydrophobic and ionizable hydrophilic monomers. In this work, we use a theoretical approach that combines the explicit description of charge regulation (acid−base equilibrium), determined by the interplay between all the physicochemical interactions described above, and the incorporation of specific molecular details of the polymer network. The basic idea of the theoretical approach is to write the free energy of the system in terms of the probability of the possible spatial conformations of the gel and include all the relevant repulsive and attractive interactions together with the different chemical states of the chargeable species. The minimization of the free energy provides the probability of each of the conformers, the state of protonation for each group, and the electrostatic as well as other interaction potentials. Thus, the theory does not assume *a priori* the state of the gel, but it rather comes as output of the minimal free energy for each set of experimentally controllable variables. The conformations of the gel are obtained from molecular dynamics simulations. The details of the molecular theory, the chain conformation generation, and the minimization procedure are presented in the Methods section and in the Supporting Information (SI).

H(i)-P(n) Hydrogel. Consider an acid−base equilibrium in a dilute solution: the fraction of deprotonated molecules, given by the degree of dissociation, f, is completely determined by the intrinsic pK_a of the isolated acid group and the solution pH, and it is given by

$$f = \frac{1}{1 + \frac{K_a}{[H^+]}} \quad (1)$$

As the pH increases two units from p$K_a - 1$ to p$K_a + 1$, the fraction of charged groups increases roughly from 10% to 90%. However, as demonstrated by Katchalsky more than 60 years ago for polyelectrolytes in solution,[52,53] and in our previous results in a variety of confined polyelectrolytes, grafted polymer layers,[50] and hydrophilic polyacid hydrogels,[49] the pK_a of the solution does not provide substantial information on the thermodynamic state in more complex systems. Here we concentrate our attention on the behavior of hydrogels of amphiphilic block copolymers, where the intrinsic pK_a of the acidic monomers is 5, and in particular on the formation of pH-dependent nanodomains.

In order to quantify the network nanostructure, we define $\Delta N_{IJ}(r)$, which gives the excess number of J-type monomers on a spherical shell of thickness dr at a distance r from a central I-type monomer, measured with respect to the case of the I-type monomer in a homogeneous solution of J-type monomers having the same average density. Namely,

$$\Delta N_{IJ}(r) = \frac{N_J}{V} V_r (g_{IJ}(r) - 1) \text{ with } \{I, J\} = \{H, P\} \quad (2)$$

where $g_{IJ}(r)$ is the I−J pair distribution function, N_J is the total number of J-type monomers in the network volume V, and V_r is the volume of the spherical shell defined by r and $r + dr$. The different panels of Figure 2 show the dependence on pH of the excess number of monomers, for hydrophobic and hydrophilic pairs of monomers. $\Delta N_{HP}(r)$ curves are not shown because they do not provide relevant additional information. The sharp peak at r = 0.5 nm represents the chemical bond between neighboring segments along the polymer chains. Hydrophilic monomers are not ionizable in this network, which explains the weak dependence of $\Delta N_{PP}(r)$ on pH. Therefore, $\Delta N_{PP}(r)$ can be used as a reference because it gives the contribution to the excess number of monomers coming from the network at the volume fraction of interest. The most interesting

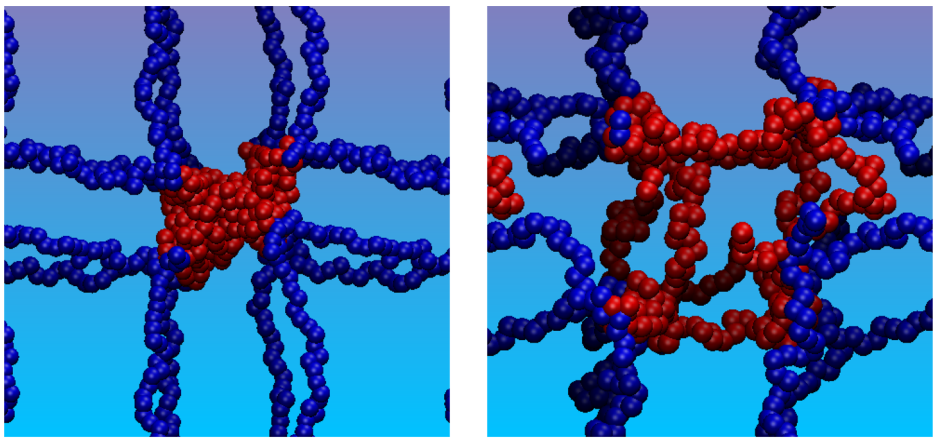

Figure 3. Conformations with maximal probability at different pH, c = 100 mM, and ϕ_G = 0.013.

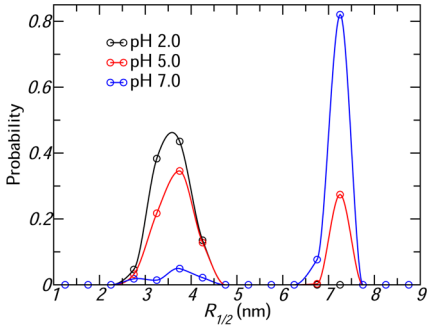

Figure 4. Probability of finding a given value of $R_{1/2}$ at different pH. The conditions correspond to the cases shown in Figure 2, c = 100 mM and ϕ_G = 0.013.

feature of Figure 2 is the different behavior found for hydrophobic monomers at different pH. At low pH, $\Delta N_{HH}(r)$ shows a large excess of hydrophobic monomers within a 5 nm distance, indicating the presence of an aggregate. The negative value of $\Delta N_{HH}(r)$ for $r >$ 5 nm, which indicates a depletion of H-monomers in this region, is also consistent with the aggregation of hydrophobic chains at $r < 5$ nm. On the other hand, the HH and PP profiles are similar to each other at high pH, indicating the swelling of the hydrophobic aggregate into water-soluble chains under this condition. Figure 3 presents the most probable, characteristic, conformations of the H(i)-P(n) network at the high and low pH cases of Figure 2. All the APCN conformations with nonzero probability at low pH are topologically similar to the low-pH conformation shown in Figure 3, while an analogous situation occurs at high pH with the other conformation displayed in the figure. Interestingly, at intermediate pH, the set of high-probability conformations contains both families of conformations and their ratio is pH dependent. The simultaneous presence of both sets of conformations, containing swollen and aggregated hydrophobic monomers, explains the less pronounced excess of monomers observed in Figure 2 (r < 5 nm) at pH 5 as compared to pH 2. To further characterize the aggregation, we define $R_{1/2}$ as the radius of a sphere that contains half of the hydrophobic monomers within the volume of the calculation. Namely,

$$\frac{4\pi}{V}\int_0^{R_{1/2}} g_{HH}(r)r^2 dr = \frac{1}{2} \qquad (3)$$

The probability distributions of $R_{1/2}$ for the same conditions of Figure 2 are displayed in Figure 4. At low pH the distribution shows one peak, which corresponds to the $R_{1/2}$ of the aggregate (~3.5 nm at this volume fraction). At constant density of hydrophobic monomers eq 3 gives $R_{1/2} = (3V/8\pi)^{1/3} = 7.08$ nm at the volume fraction we are considering. Thus, at high pH, although the aggregate has a nonzero probability, the most significant part of the distribution centers around a value of $R_{1/2}$ that corresponds to a swollen domain. Low, intermediate, and high pH are defined in terms of whether the network is uncharged, weakly charged, or strongly charged, respectively. These different regimes are quantified using the weighted average degree of dissociation of ionizable monomers,

$$\langle f_d \rangle = \frac{\int d\mathbf{r} \langle \phi^{IP}(\mathbf{r}) \rangle f_d(\mathbf{r})}{\int d\mathbf{r} \langle \phi^{IP}(\mathbf{r}) \rangle}$$

where $\langle \phi^{IP}(\mathbf{r}) \rangle$ is the (ensemble average) local volume fraction of ionizable polymer and $f_d(\mathbf{r})$ is the local degree of dissociation, which is 0.001, 0.30, and 0.97 for the cases shown in Figures 2 and 4 at pH 2, 5, and 7, respectively. At pH 5 Figure 4 shows a bimodal probability distribution of $R_{1/2}$, indicating that both conformations of the hydrophobic chains, aggregated (low $R_{1/2}$) and swollen (high $R_{1/2}$), have significant probabilities. The bimodal distribution suggests microphase separation in the APCN between domains of swollen and aggregated hydrophobic chains.

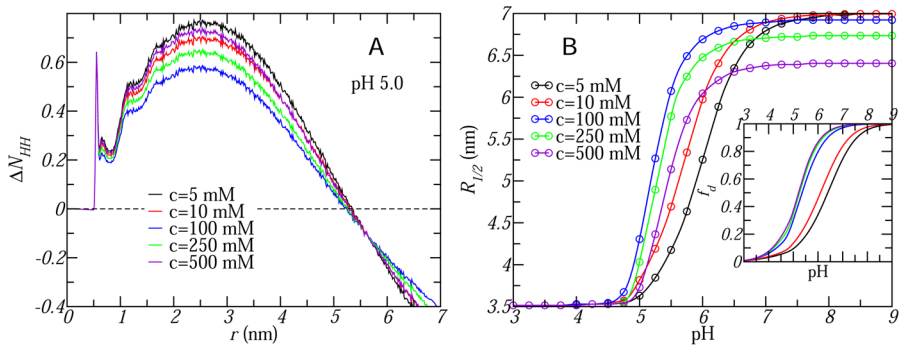

Figure 5. $\Delta N_{HH}(r)$ at bath pH 5 (A) and $R_{1/2}$ as a function of pH (B) at different salt concentrations, $\phi_G = 0.013$. The inset of panel B shows the pH-dependence of the average degree of dissociation at the same conditions.

The behavior of the APCN aggregate under different ionic strengths is presented in Figure 5, where panel A shows the excess number of hydrophobic monomer pairs for different salt concentrations, at constant volume fraction and pH. The bath pH has been chosen to be equal to the intrinsic pK_a of the acidic monomers (pH = pK_a = 5.0), which corresponds to the intermediate pH range; at lower pH, the dependence of $\Delta N_{HH}(r)$ on salt concentration is weaker, while at higher values of pH the presence of the aggregate is thermodynamically much less favorable. The hydrophobic aggregate forms due to the solvophobic attractions between those monomers. However, it is the competition between chemical equilibrium and the physical interactions that determine the thermodynamic structure of the network. For pH near or above pK_a, the acid−base equilibrium favors deprotonation, which has an energetic cost due to the stronger electrostatic repulsions between the charged monomers. If such repulsions become sufficiently strong, the hydrophobic chains will swell to reduce the electrostatic interactions, at the cost of reducing the hydrophobic attractions, and the formation of the aggregate will be unfavorable. Increasing the salt concentration of the solution has a dual effect on the electrostatic repulsions. On the one hand, there is a larger screening of the interactions between charged monomers, which reduces the effective range of the repulsions. Namely, the Debye length of the solution, λ_D, which gives a measure of effective extent of the electrostatic interactions between charged monomers, decreases, thus diminishing the importance of the electrostatic repulsions relative to the hydrophobic attractions. Therefore, screening of the electrostatic repulsions leads to a higher probability for the formation of the hydrophobic aggregate. On the other hand, a shorter λ_D allows for an increase in the degree of dissociation, which is strongly favored by the acid−base equilibrium, increasing the electrostatic repulsions and decreasing the probability for nanoaggregation.

The degree of dissociation in the cases shown in Figure 5A are $\langle f_d \rangle$ is 0.09, 0.13, 0.30, 0.35, and 0.37 for c = 5, 10, 100, 250, and 500 mM, respectively; at pH = pK_a, where the degree of dissociation of the isolated acid group in bulk solution would be 1/2. We see that increasing the solution ionic strength at fixed pH increases the degree of dissociation of the acid monomers of the gel. Interestingly, even at the highest salt concentration the dissociation is significantly lower than in bulk solution due to the role of local electrostatic repulsion in shifting the acid−base equilibrium. One very clear manifestation of the dual role of salt concentration and of its coupling with other interactions and molecular organization is the fact that the maximum in ΔN_{HH} ($r \approx 2.5$ nm, excluding the monomer chemical bonds) is a nonmonotonic function of the salt concentration. Aggregation is favored by less charge in the acidic monomers; however more charge does not necessarily result in larger electrostatic repulsions when the salt concentration changes.

Figure 5B shows $R_{1/2}$ as a function of pH for different salt concentrations, at constant volume fraction. The formation of the hydrophobic aggregate with $R_{1/2}$ = 3.5 nm is clearly observed at low pH. The size of the aggregate is independent of the solution ionic strength since the network is uncharged ($\langle f_d \rangle \approx 0$), and therefore hydrophobic attractions are the only dominant interactions. At high pH the hydrogel is strongly charged ($\langle f_d \rangle > (1/2)$) and the electrostatic repulsions are the most significant contribution to the free energy. The magnitude of $R_{1/2}$ in the high pH range indicates that the hydrophobic chains are swollen. The degree of swelling at high pH is a monotonic increasing function of salt concentration, demonstrating that the most relevant interactions are the purely electrostatic repulsions between the charged groups. However, the value of the high-pH plateau depends on the solution ionic strength, which can also be understood in terms of the Debye length of the solution, namely, on the range of the electrostatic interactions. For the two lowest salt concentrations the Debye length is of the magnitude of the fully swollen chains, and thus the hydrophobic attractions play no role. At the other three ionic strengths the decrease in the size of the charged hydrophobic swollen domains is the result of the attractions starting to play a (minor) role.

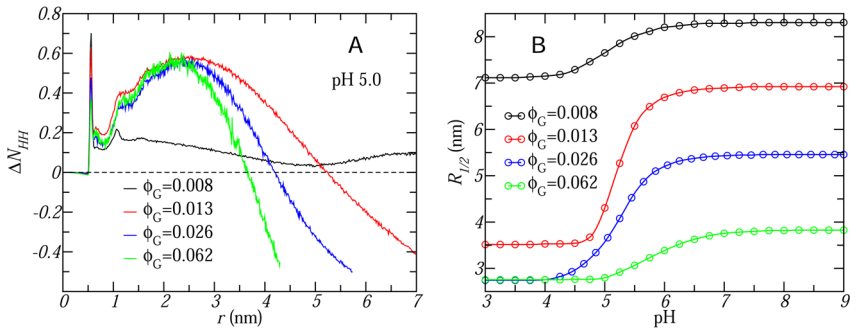

Figure 6. $\Delta N_{HH}(r)$ at pH 5 (A) and $R_{1/2}$ as a function of pH (B) at different volume fractions and c = 100 mM.

An interesting nonmonotonic dependence of the nanodomain size on salt concentrations is observed at intermediate pH. First, the width of the transition from aggregated to swollen is a function of salt concentration. This is a direct manifestation of the dependence of the degree of dissociation on pH, as shown in the inset of Figure 5B. $\langle f_d \rangle$ has a broader pH-dependent transition from the uncharged (∼0) to the fully dissociated regime (∼1) as the salt concentration decreases. The width of the pH region in which such transition occurs can be quantified using $\Delta pH = pH_1 - pH_0$, where $\langle f_d \rangle = (1/11)(\sim 0.1)$ when $pH = pH_0$, and $\langle f_d \rangle = (10/11)(\sim 0.9)$ when $pH = pH_1$. ΔpH is exactly 2 for the deprotonation of the isolated acid group in a dilute solution with no salt. For the APCN at constant volume fraction ΔpH always increases with decreasing ionic strength (see inset of Figure 5B and Figure S2 of the SI); this effect is similar to that observed in charged biopolymers.[52,53] However, at intermediate pH $R_{1/2}$ shows a nonmonotonic dependence on c. Similarly to that observed in Figure 5A, this behavior is the consequence of the dual effect that increasing salt concentration has on the strength of the electrostatic repulsions and consequently on the competition between the electrostatic repulsions and the hydrophobic attractions that lead to domain formation. Interestingly these results suggest that one can control the microphase separation region, *i.e.*, where the aggregated and swollen domains coexist (Figure 4), with pH and ionic strength.

The polymer volume fraction limits the average end-to-end distance of hydrophobic chains and thus the formation of the aggregate. Figure 6A and B illustrate the behavior of the hydrophobic chains for different total polymer volume fractions. At the lowest volume fraction, the polymer chains are highly stretched, which limits the flexibility of the network and prevents the hydrophobic monomers from aggregating at all pH's. For higher volume fractions the formation of an aggregate is clearly observed. As the volume fraction increases, the average end-to-end distance of hydrophobic chains decreases, which favors the formation of the aggregate and explains why the size of the aggregate at low pH is the same for the two highest volume fractions shown in Figure 6B. Indeed, increasing the volume fraction by almost an order of magnitude to $\phi_G = 0.21$ yields $R_{1/2} \approx 2.5$ nm at low pH, which indicates the presence of an aggregate of similar size to that obtained for the highest volume fraction shown in Figure 6B. The role of volume fraction is clearly manifested in the balance between chemical equilibrium and physical interactions. In other words, at constant pH an increase in volume fraction disfavors deprotonation due to the short distance between monomers, *i.e.*, increasing electrostatic repulsions. At $pH = pK_a = 5$, for example, the average degrees of dissociation are 0.21, 0.29, 0.30 and 0.38, for $\phi_G = 0.062$, 0.026, 0.013, and 0.008, respectively.

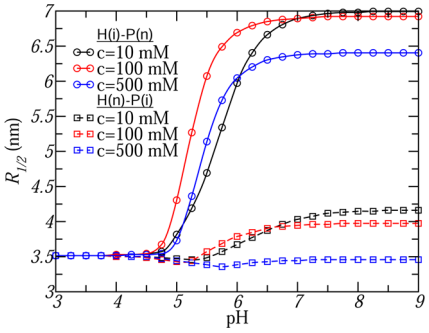

Figure 7. $R_{1/2}$ as a function of pH for the two APCN, H(i)-P(n) (circles, solid lines) and H(n)-P(i) (squares, dashed lines), at different salt concentrations; ϕ_G = 0.013.

H(i)-P(n) *vs* H(n)-P(i) Hydrogels. In this section we compare the molecular structures of the H(i)-P(n) network with ionizable hydrophobic monomers, characterized in the previous section, with a H(n)-P(i) network where the hydrophilic monomers are ionizable. Except for the position of the acidic groups the molecular architectures of the two hydrogels are identical. We will show that although the macroscopic responses of the two networks are similar, their behaviors are substantially different at the nanometer scale.

We begin by characterizing the response of the hydrophobic chains to changes in the bath pH. $R_{1/2}$ as a function of pH at different salt concentrations and constant volume fraction is displayed in Figure 7. For the H(n)-P(i) APCN the formation of a hydrophobic

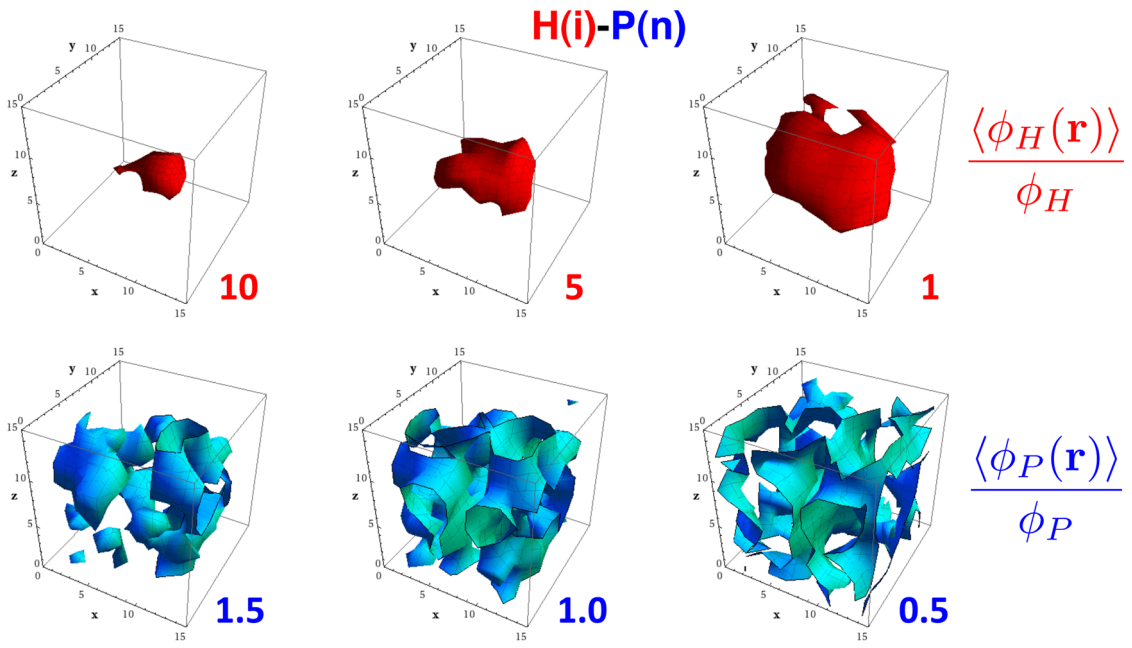

Figure 8. Surfaces of constant volume fraction of hydrophobic (top) and hydrophilic (bottom) polymer of the H(i)-P(n) network at c = 100 mM, pH 5, and ϕ_G = 0.013. The magnitude of the various isosurfaces for both types of polymer can be directly compared because $\phi_P = \phi_H = (\phi_G/2)$. The Cartesian coordinates are in nm.

aggregate is found to be favorable in the entire range of bath pH and c studied. The probability of swollen conformations of the hydrophobic chains is relatively small, and it depends only weakly on the bath solution composition. The H(n)-P(i) hydrophobic monomers do not bear an acidic group, and thus, the dependence on pH of the conformation adopted by these chains is indirect. At high pH the swelling of the charged hydrophilic chains constrains the end-to-end distance of hydrophobic chains, which leads to a slightly higher probability of the swollen hydrophobic chains ($R_{1/2}$ increases), except at high c. At the volume fraction of the figure, the swelling of the hydrophilic chains due to increasing pH imposes only a weak constraint on the formation of the hydrophobic aggregate. Actually, increasing the pH for the highest salt concentration results in a higher probability of the hydrophobic aggregate (*i.e.*, $R_{1/2}$ decreases). The dual effect of increasing salt concentration is observed in the nonmonotonic dependence of $R_{1/2}$ on c in the region between pH 5 and 7. The important result is that while we observe the different competitions described above for H(n)-P(i), the effects are rather small, a major difference from the behavior of the H(i)-P(n) networks.

To obtain a more detailed description of the structure of the networks, we show in Figure 8 three-dimensional maps of surfaces of constant local volume fraction for hydrophobic, $\langle\phi_H(\mathbf{r})\rangle$, and hydrophilic, $\langle\phi_P(\mathbf{r})\rangle$, monomers for the H(i)-P(n) architecture. The local volume fractions are normalized by the average volume fraction of the monomer type in the network. Thus, values higher (lower) than 1 imply locally enhanced (depleted) densities of monomers. The presence of the hydrophobic aggregate is clearly observed in the compact and high value of the $\langle\phi_H(\mathbf{r})\rangle/\phi_H$ isosurfaces, while the hydrophilic polymer is more homogeneously distributed across the volume of the system, although it is excluded from the region of highest density of hydrophobic monomers.

Figures 9 and 10 present surfaces of constant local pH and constant density of charge on the network for the two architectures of APCNs considered. The local pH inside the APCN is defined as $\mathrm{pH}(\mathbf{r}) = -\log([H^+](\mathbf{r}))$, where $\mathbf{r}$ is the position vector and $[H^+](\mathbf{r})$ is the local concentration of protons in molar units. The (ensemble average) local density of charge on the polymer network is $\langle\rho_q^{IP}(\mathbf{r})\rangle$, where the superscript IP refers to the ionizable polymer: IP = H for the H(i)-P(n) architecture, and IP = P for the H(n)-P(i) structure. The conditions of both Figures 9 and 10 are the same as those of Figure 8: the bath pH is 5, c = 100 mM, and ϕ_G = 0.013.

Figures 8 and 9 indicate that the density of electric charge on the polymer network is correlated with higher density of hydrophobic polymer for the H(i)-P(n) network. This is expected since the hydrophobic monomer is the one modified with acidic groups. However, one needs also to consider that, as discussed above, the acid−base equilibrium shifts to the unprotonated species in regions of high acid-monomer concentration. Both things are true; the local degree of dissociation $f_d(\mathbf{r})$ decreases significantly in the regions of high monomer concentration (see Figure S3 in the SI), which clearly indicates that aggregation disfavors deprotonation in the H(i)-P(n) network.

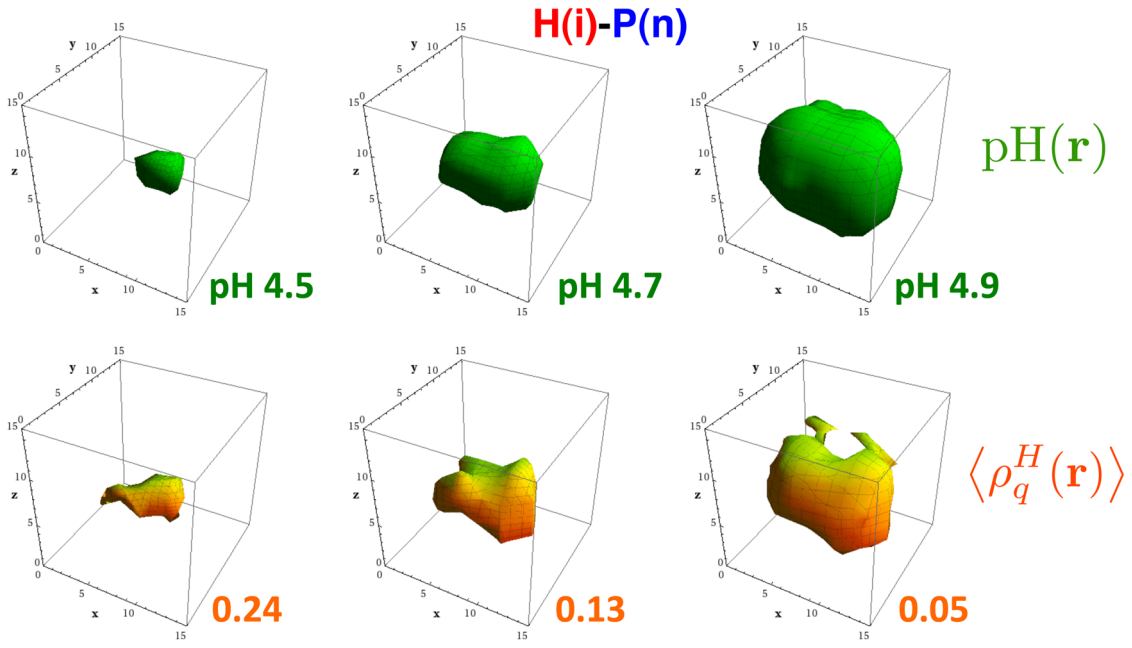

Figure 9. Isosurfaces of local pH (top) and local density of charge on the polymer backbone (bottom) of the H(i)-P(n) architecture at c = 100 mM, pH 5, and ϕ_G = 0.013. $\langle \rho_q^H(\mathbf{r}) \rangle$ is in units of e nm^{-3} (e is the electron charge), and the Cartesian coordinates are in nm.

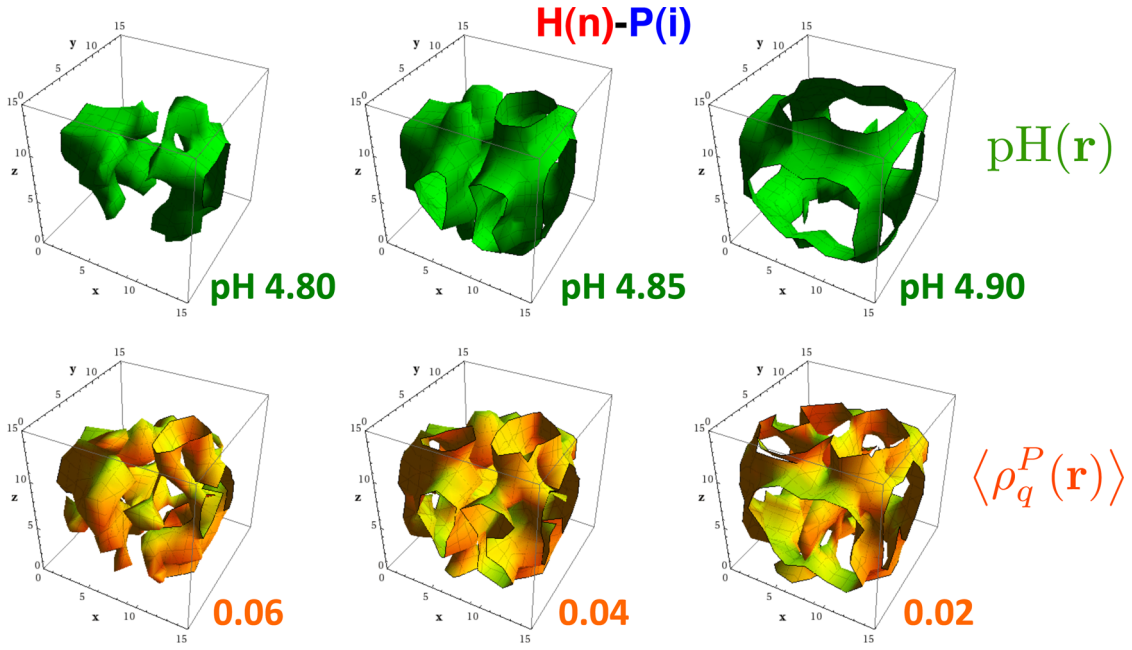

Figure 10. Isosurfaces of local pH (top) and local charge density on the polymer backbone (bottom) of the H(n)-P(i) architecture at c = 100 mM, pH 5, and ϕ_G = 0.013. $\langle \rho_q^P(r) \rangle$ is in units of e nm^{-3}, and the Cartesian coordinates are in nm.

The product of the degree of dissociation by the local density of hydrophobic monomers provides the local charge. It is interesting to note the importance of considering the local variation of the different properties in understanding the responsiveness of these polymer networks. For example, the average degree of dissociation for the case in Figures 8 and 9 and Figure S3 is $\langle f_d \rangle$ = 0.30; however, in the surface where $\langle \rho_q^H(r) \rangle$ = 0.24e nm^{-3}, $f_d(\mathbf{r})$ = 0.22, while in the region where $\langle \rho_q^H(r) \rangle$ = 0.05e nm^{-3}, $f_d(\mathbf{r})$ = 0.4. This implies that drawing conclusions from average values of the network may be misleading since the local arrangement is highly inhomogeneous. At higher pH than the one just discussed, the aggregates swell to redistribute the increasing electric charge more homogeneously across the volume. Moreover, to further highlight the importance of molecular architecture, we will show that in the H(n)-P(i) architecture

the electric charge is more spread across the system volume, which allows for a higher degree of dissociation.

The negative charge on the network backbone induces a recruitment of mobile positive ions to locally balance the electric charge, which explains the inverse correlation between isosurfaces of local pH and those of density of network charge observed in Figure 9. As an interesting consequence, constant-pH surfaces are controlled by the formation of the hydrophobic aggregate, and the lowest pH is obtained in the region of highest density of hydrophobic polymer, which has the highest network charge density.

The nanostructure of the H(n)-P(i) network at pH 5 is described in Figure S4 of the SI. The surfaces of constant-volume fraction of both types of polymer are qualitatively similar to those of the H(i)-P(n) network shown in Figure 8: compact and high-magnitude isosurfaces of volume fraction of hydrophobic polymer are obtained, which indicates the presence of the aggregate, while the hydrophilic polymer is spread across the volume. We have also found that surfaces of constant density of hydrophobic monomers are very similar for both architectures at lower pH. At higher pH, however, the aggregate is still present in the H(n)-P(i) APCN, provided that the polymer volume fraction is high enough, but vanishes for the H(i)-P(n) network, as discussed in Figure 7.

The electric charge on the network is distributed more homogeneously across the volume for the H(n)-P(i) structure, Figure 10, as compared to the H(i)-P(n), Figure 8. This is because in the former case the acidic groups are on the hydrophilic polymer, and isosurfaces of increasing density of such polymer are correlated with those of higher density of charge on the network. In addition, the more spread distribution of network charge explains the higher average degree of dissociation in the structure with ionizable hydrophilic polymer: $\langle f_d \rangle = 0.37$ at the conditions of Figure 10, as opposed to $\langle f_d \rangle = 0.30$ for the H(i)-P(n) at the same conditions.

We define pH_{GEL} as the volume average of the local pH inside the APCN. For the cases of Figures 9 and 10 $pH_{GEL} = 4.87$, for the H(n)-P(i) network, and $pH_{GEL} = 4.90$, for the H(i)-P(n) network. The lower pH in the network with ionizable hydrophilic polymer is due to the higher degree of charge in that structure. However, pH_{GEL}, which gives the average pH inside the hydrogel, is not a very significant quantity for the H(i)-P(n) network since the local pH changes dramatically in different regions of the hydrogel. For example, changes of up to half a pH unit within 5 nm are observed at the conditions of intermediate pH, as shown in Figure 9. The formation of the aggregate results in the localization of the negative electric charge on the H(i)-P(n) network, which generates a sharp gradient of positive mobile ions with potential applications for ion transport.

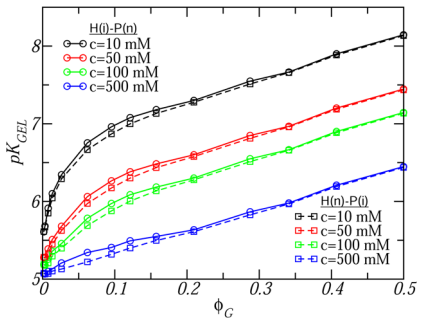

Figure 11. Apparent pK_a *vs* volume fraction at different salt concentrations. Results for both APCNs: H(i)-P(n) (circles, solid lines) and H(n)-P(i) (squares, dashed lines), are shown.

If the volume of the APCN is not constrained, the optimal volume fraction of the gel would be that which minimizes the free energy of the system at the given bath pH and *c*. The optimal volume of both types of APCNs shows an almost identical dependence on the pH and ionic strength (see Figure S6 in the SI). At low pH the hydrogel is in a collapsed, high-volume fraction, state. As the pH increases the network transitions from the collapsed state to a swollen, low-volume fraction, state. The swelling starts to occurs at relatively low pH values (depending on salt concentration), and it is completed close to the bulk pK_a. The width of the pH region in which the network transitions from collapsed to swollen depends critically on the salt concentration. The smaller the ionic strength is, the sharper the transition (see Figure S6 in the SI); for example at c = 10 mM the transition occurs in one pH unit, while at c = 100 mM it spreads through two units. This swelling response as pH and c change is analogous to the behavior described in our previous work for a poly(acrylic acid) hydrogel.[49]

Another quantity that can be used to describe the macroscopic behavior of the APCNs is pK_{GEL}, the apparent pK_a of the APCN. pK_{GEL} is defined as the bath pH at which, on average, half of the ionizable monomers are deprotonated (*i.e.*, $\langle f_d \rangle_{pH=pK_{GEL}} = 1/2$). The apparent p$K_a$ as a function of the total polymer volume fraction for both of the APCNs considered is presented in Figure 11, at different salt concentrations. At constant volume fraction, it always requires a slightly higher pH to strongly charge ($f_d \geq 1/2$) the hydrophobic monomers in the H(i)-P(n) network than it does to strongly ionize the hydrophilic monomers in the H(n)-P(i) hydrogel. However, the differences in pK_{GEL} between the two APCNs are small compared to displacement from the solution behavior (pK_a) introduced by the presence of the network. The macroscopic behaviors of the two architectures, characterized by both the swelling transition and the apparent pK_a, are quantitatively similar, while the behaviors of the networks at the nanoscale are qualitatively different. A macroscopic measure such as pK_{GEL} is not an appropriate quantity to describe the structure of the gel.

This may have important consequences for the molecular design of responsive hydrogels, *e.g.*, in oral drug delivery applications that require control over the structure and local environment of the hydrogel host, in particular in light of the dramatic differences and large gradients found in the local pH, charge density, and more, described in connection with Figures 8 to 10.

CONCLUSION

In this study, we have described the responsive behavior and nanoscale structure of two APCNs with different molecular structures as a function of the salt concentration and pH of the solution in equilibrium with the network. We have considered a regular molecular model of the amphiphilic network. In the H(i)-P(n) network, the hydrophobic monomers bear acidic groups, while the hydrophobic monomers are not ionizable. In the H(n)-P(i) network, the hydrophilic monomers are the ones modified with acidic groups, and the hydrophobic monomers are nonionizable. The pK_a of the ionizable monomers is the same in both cases. Even for this simple molecular model of APCN, the nanoscopic behavior shows several interesting features. If the hydrophobic monomers are ionizable, their aggregation is controlled by the bath pH. At low pH, a hydrophobic aggregate is found. Increasing pH reduces the probability of finding such an aggregate until that probability becomes negligible at high pH. At intermediate pH, our results indicate that the APCN separates into microphases of swollen and aggregated hydrophobic chains. Except at low pH, the most likely conformation of the hydrophobic chains depends on the solution ionic strength. When the pH is near or above the intrinsic pK_a of the ionizable monomers, the chemical free energy favors a substantial increase in the degree of dissociation of the network. However, the electrostatic energy favors a low degree of charge to minimize the repulsions between charged monomers. Strong electrostatic repulsions oppose the aggregation of charged hydrophobic monomers.

The addition of salt to the solution has a dual effect. On one hand, there is a larger screening of the electrostatic interactions, which reduces the effective range and strength of the repulsions between charged monomers, favoring the aggregation of hydrophobic monomers. On the other hand, a shorter Debye length enables a higher degree of dissociation, which increases the strength of the intranetwork electrostatic repulsions, leading to swelling of the hydrophobic aggregate. These two competing effects have the most significant consequences at intermediate pH, that is, when the degree of dissociation is neither high nor close to zero ($0 \ll \langle f_d \rangle < 1/2$). For this reason, the probability of finding the aggregate shows a nonmonotonic dependence on c within this pH range. At low pH, the degree of dissociation is close to zero and the electrostatic repulsions are weak, which results in the behavior of the hydrophobic chains being independent of salt concentration. Moreover, at high pH, the network electrostatic repulsions are already strong due to the high degree of dissociation, and only the effect of increased screening is significant. When the hydrophilic polymer is ionizable, the nanoaggregation of hydrophobic chains is less sensitive to environment changes because the stimulus occurs indirectly due to network connectivity interactions. Therefore, except at very low network volume fraction, the aggregate is the most likely conformation of the hydrophobic chains at all pH and salt concentrations.

The environment pH can be used to control the nanoaggregation of hydrophobic monomers in a H(i)-P(n) APCN. This finding has potential for applications in controlled oral delivery of hydrophobic drugs that can be loaded by contact with a high-pH solution containing the molecule to deliver. As the pH is reduced, the drug will be entrapped in the collapsing hydrophobic regions of the network, and release occurs by diffusion at the high-pH target environment when the hydrophobic chains are most likely swollen due to their increasing degree of ionization. The H(i)-P(n) network performs local mechanical work, which occurs at overall constant total volume of the hydrogel, in response to changes in the chemical composition of the environment. This work given by the contracting and relaxing of the hydrophobic regions of the network can be exploited in the development of devices such as artificial muscles.

The macroscopic responses (*i.e.*, swelling behavior and network apparent pK_a) of the H(n)-P(i) and H(i)-P(n) APCNs are similar. However, at the nanoscale the hydrogels behave very differently. Inside the H(i)-P(n) network, well-defined, confined pH and polymer density of charge isosurfaces are observed at a bath pH where the aggregation is favorable. These surfaces are highly correlated with the surfaces of equal density of hydrophobic monomer, which is in this case the ionizable monomer. The variability of pH (or the polymer charge density) inside this network is also higher than it is in the H(n)-P(i) APCN. In the latter network, isosurfaces of pH and polymer charge density follow the surfaces of constant volume fraction of hydrophilic polymer, which contains the ionizable monomers. As a consequence, these surfaces are not confined but extend across the volume of the network, or more precisely, they span the entire volume complementary to that of the hydrophobic aggregate. Therefore, the molecular design of the network can be used to control the local charge distribution inside the hydrogel, even for regular structures such as the one considered in this study. In most applications of pH-responsive hydrogels, molecular design is generally used to control the swelling properties of the network. Appropriate choice

of the molecular architecture of APCN, however, can help engineer novel applications that go beyond the use of hydrogels as simple sweallable templates, in which local domains and large gradient of charge and pH can be used to optimize the state of host molecules, *e.g.*, drugs, and their release to the environment. Molecular design of the APCN allows localizing the charge distribution within the network structure as well as controlling the distribution of chemical species within the hydrogel.

METHODS

To describe the thermodynamic behavior of the APCN, we use a molecular theory that accounts for specific details of the polymer network. The molecular conformations of the network are incorporated into the approach using MD simulations. One of the salient characteristics of this molecular-level theory is that it explicitly describes charge self-regulation, which is the distinguishing feature of most stimuli-responsive hydrogels. The first step in this theoretical framework consists in writing the total free energy of the APCN, which is given by

$$F = -TS_{conf} - TS_{mix} + U_{vdw} + U_{st} + F_{chm} + U_{elec} \quad (4)$$

where T is the system temperature, S_{conf} is the conformational entropy of the flexible network, S_{mix} is the translational entropy of the different free species in the solution, U_{vdw} is total attractive van der Waals interaction, U_{st} is the total repulsive steric (excluded volume) interaction, F_{chm} is the chemical free energy that accounts for the acid−base equilibrium, and U_{elec} is the total electrostatic energy. Each of these terms of the free energy can be explicitly expressed as a functional of the probability of the different molecular conformations of the network, the local density profiles of the mobile species in the solution, the local degree of dissociation of the ionizable polymer, and the electrostatic potential. The next step is to optimize the free energy functional with respect to each of these functions, which leads to a series of equations that are solved numerically. All structural properties can be determined from the probabilities and interaction fields obtained from the minimized free energy, and any thermodynamic quantity of interest can be computed by taking the proper derivative of the minimized thermodynamic potential. Technical details and all the relevant equations of the molecular theory can be found in the SI and in our previous work.[49]

Conflict of Interest: The authors declare no competing financial interest.

Supporting Information Available: Thorough description of the general molecular theory of pH-responsive hydrogels, its application to APCNs, and its numerical implementation. Details of the molecular model of APCN considered in this work. Additional results not included in this article. This material is available free of charge *via* the Internet at http://pubs.acs.org.

Acknowledgment. M.O.C. acknowledges support from NSF (DMR-0907781). Collaboration for AIDS Vaccine Discovery grant to I.S. from the Bill and Melinda Gates Foundation (OPP1031734, PI: T. Hope) is also acknowledged.

REFERENCES AND NOTES

1. Chen, G.; Hoffman, A. S. Graft Copolymers That Exhibit Temperature-Induced Phase Transitions over a Wide Range of pH. *Nature* **1995**, *373*, 49–52.
2. Yoshida, R.; Uchida, K.; Kaneko, Y.; Sakai, K.; Kikuchi, A.; Sakurai, Y.; Okano, T. Comb-Type Grafted Hydrogels with Rapid Deswelling Response to Temperature Changes. *Nature* **1995**, *374*, 240–242.
3. Tanaka, T.; Nishio, I.; Sun, S.-T.; Ueno-Nishio, S. Collapse of Gels in an Electric Field. *Science* **1982**, *218*, 467–469.
4. Kwon, I. C.; Bae, Y. H.; Kim, S. W. Electrically Credible Polymer Gel for Controlled Release of Drugs. *Nature* **1991**, *354*, 291–293.
5. Osada, Y.; Okuzaki, H.; Hori, H. A Polymer Gel with Electrically Driven Motility. *Nature* **1992**, *355*, 242–244.
6. Kaneko, D.; Gong, J. P.; Osada, Y. Polymer Gels As Soft and Wet Chemomechanical Systems−An Approach to Artificial Muscles. *J. Mater. Chem.* **2002**, *12*, 2169–2177.
7. Suzuki, A.; Tanaka, T. Phase Transition in Polymer Gels Induced by Visible Light. *Nature* **1990**, *346*, 345–347.
8. Matsuo, E. S.; Tanaka, T. Patterns in Shrinking Gels. *Nature* **1992**, *358*, 482–485.
9. Mccoy, J. L.; Muthukumar, M. Dynamic Light Scattering Studies of Ionic and Nonionic Polymer Gels with Continuous and Discontinuous Volume Transitions. *J. Polym. Sci., Part B: Polym. Phys.* **2010**, *48*, 2193–2206.
10. Tanaka, T.; Fillmore, D.; Sun, S.-T.; Nishio, I.; Swislow, G.; Shah, A. Phase Transitions in Ionic Gels. *Phys. Rev. Lett.* **1980**, *45*, 1636–1639.
11. Zhao, B.; Moore, J. S. Fast pH- and Ionic Strength-Responsive Hydrogels in Microchannels. *Langmuir* **2001**, *17*, 4758–4763.
12. De, S.; Aluru, N.; Johnson, B.; Crone, W.; Beebe, D.; Moore, J. Equilibrium Swelling and Kinetics of pH-Responsive Hydrogels: Models, Experiments, and Simulations. *J. Microelectromech. Syst.* **2002**, *11*, 544–555.
13. Ulijn, R. V. Enzyme-Responsive Materials: A New Class of Smart Biomaterials. *J. Mater. Chem.* **2006**, *16*, 2217–2225.
14. Zhang, Y.-Q.; Tanaka, T.; Shibayama, M. Super-Absorbency and Phase Transition of Gels in Physiological Salt Solutions. *Nature* **1992**, *360*, 142–144.
15. Song, J. Y.; Wang, Y. Y.; Wan, C. C. Review of Gel-Type Polymer Electrolytes for Lithium-Ion Batteries. *J. Power Sources* **1999**, *77*, 183–197.
16. Beebe, D. J.; Moore, J. S.; Bauer, J. M.; Yu, Q.; Liu, R. H.; Devadoss, C.; Jo, B.-H. Functional Hydrogel Structures for Autonomous Flow Control inside Microfluidic Channels. *Nature* **2000**, *404*, 588–590.
17. Kim, P.; Zarzar, L. D.; Zhao, X.; Sidorenko, A.; Aizenberg, J. Microbristle in Gels: Toward All-Polymer Reconfigurable Hybrid Surfaces. *Soft Matter* **2010**, *6*, 750–755.
18. Suzuki, M.; Hirasa, O.; Dušek, K. An Approach to Artificial Muscle Using Polymer Gels Formed by Micro-Phase Separation. *Adv. Polym. Sci.* **1993**, *110*, 241–261.
19. Shahinpoor, M. Micro-Electro-Mechanics of Ionic Polymeric Gels As Electrically Controllable Artificial Muscles. *J. Intell. Mater. Syst. Struct.* **1995**, *6*, 307–314.
20. Sidorenko, A.; Krupenkin, T.; Taylor, A.; Fratzl, P.; Aizenberg, J. Reversible Switching of Hydrogel-Actuated Nanostructures into Complex Micropatterns. *Science* **2007**, *315*, 487–490.
21. Kopecek, J. Hydrogel Biomaterials: A Smart Future? *Biomaterials* **2007**, *28*, 5185–5192.
22. Torres-Lugo, M.; Peppas, N. A. Molecular Design and *in Vitro* Studies of Novel pH-Sensitive Hydrogels for the Oral Delivery of Calcitonin. *Macromolecules* **1999**, *32*, 6646–6651.
23. Qiu, Y.; Park, K. Environment-Sensitive Hydrogels for Drug Delivery. *Adv. Drug Delivery Rev.* **2001**, *53*, 321–339.
24. Vinogradov, S. V.; Bronich, T. K.; Kabanov, A. V. Nanosized Cationic Hydrogels for Drug Delivery: Preparation, Properties and Interactions with Cells. *Adv. Drug Delivery Rev.* **2002**, *54*, 135–147.
25. Lee, K. Y.; Mooney, D. J. Hydrogels for Tissue Engineering. *Chem. Rev.* **2001**, *101*, 1869–1880.
26. Ehrick, J. D.; Luckett, M. R.; Khatwani, S.; Wei, Y.; Deo, S. K.; Bachas, L. G.; Daunert, S. Glucose Responsive Hydrogel Networks Based on Protein Recognition. *Macromol. Biosci.* **2009**, *9*, 864–868.
27. Wu, W.; Mitra, N.; Yan, E. C. Y.; Zhou, S. Multifunctional Hybrid Nanogel for Integration of Optical Glucose Sensing

and Self-Regulated Insulin Release at Physiological pH. *ACS Nano* **2010**, *4*, 4831–4839.
28. Brannon-Peppas, L.; Peppas, N. A. Dynamic and Equilibrium Swelling Behaviour of pH-Sensitive Hydrogels Containing 2-Hydroxyethyl Methacrylate. *Biomaterials* **1990**, *11*, 635–644.
29. Bettini, R.; Colombo, P.; Peppas, N. A. Solubility Effects on Drug Transport through pH-Sensitive, Swelling-Controlled Release Systems: Transport of Theophylline and Metoclopramide Monohydrochloride. *J. Controlled Release* **1995**, *37*, 105–111.
30. am Ende, M. T.; Peppas, N. A. Transport of Ionizable Drugs and Proteins in Crosslinked Poly(acrylic acid) and Poly(Acrylic Aid-co-2-Hydroxyethyl Methacrylate) Hydrogels. II. Diffusion and Release Studies. *J. Controlled Release* **1997**, *48*, 47–56.
31. Liechty, W. B.; Caldorera-Moore, M.; Phillips, M. A.; Schoener, C.; Peppas, N. A. Advanced Molecular Design of Biopolymers for Transmucosal and Intracellular Delivery of Chemotherapeutic Agents and Biological Therapeutics. *J. Controlled Release* **2011**, *155*, 119–127.
32. Hoare, T. R.; Kohane, D. S. Hydrogels in Drug Delivery: Progress and Challenges. *Polymer* **2008**, *49*, 1993–2007.
33. Inoue, T.; Chen, G.; Nakamae, K.; Hoffman, A. S. A Hydrophobically-Modified Bioadhesive Polyelectrolyte Hydrogel for Drug Delivery. *J. Controlled Release* **1997**, *49*, 167–176.
34. Patrickios, C. S.; Georgiou, T. K. Covalent Amphiphilic Polymer Networks. *Curr. Opin. Colloid Interface Sci.* **2003**, *8*, 76–85.
35. Erdodi, G.; Kennedy, J. P. Amphiphilic Co-networks: Definition, Synthesis, Applications. *Prog. Polym. Sci.* **2006**, *31*, 1–18.
36. Nicolson, P. C.; Vogt, J. Soft Contact Lens Polymers: An Evolution. *Biomaterials* **2001**, *22*, 3273–3283.
37. Gudipati, C. S.; Greenlief, C. M.; Johnson, J. A.; Prayongpan, P.; Wooley, K. L. Hyperbranched Fluoropolymer and Linear Poly(Ethylene Glycol) Based Amphiphilic Crosslinked Networks As Efficient Antifouling Coatings: An Insight into the Surface Compositions, Topographies, and Morphologies. *J. Polym. Sci., Part A: Polym. Chem.* **2004**, *42*, 6193–6208.
38. Tiller, J. C.; Sprich, C.; Hartmann, L. Amphiphilic Conetworks As Regenerative Controlled Releasing Antimicrobial Coatings. *J. Controlled Release* **2005**, *103*, 355–367.
39. Barakat, I.; Dubois, P.; Grandfils, C.; Jérôme, R. Macromolecular Engineering of Polylactones and Polylactides. XXV. Synthesis and Characterization of Bioerodible Amphiphilic Networks and Their Use As Controlled Drug Delivery Systems. *J. Polym. Sci., Part A: Polym. Chem.* **1999**, *37*, 2401–2411.
40. Haigh, R.; Fullwood, N.; Rimmer, S. Synthesis and Properties of Amphiphilic Networks 2: A Differential Scanning Calorimetric Study of Poly(Dodecyl Methacrylate-stat-2,3 Propandiol-1-Methacrylate-stat-Ethandiol Dimethacrylate) Networks and Adhesion and Spreading of Dermal Fibroblasts on These Materials. *Biomaterials* **2002**, *23*, 3509–3516.
41. Bruns, N.; Tiller, J. C. Amphiphilic Network As Nanoreactor for Enzymes in Organic Solvents. *Nano Lett.* **2004**, *5*, 45–48.
42. Kang, Y.; Walish, J. J.; Gorishnyy, T.; Thomas, E. L. Broad-Wavelength-Range Chemically Tunable Block-Copolymer Photonic Gels. *Nat. Mater.* **2007**, *6*, 957–960.
43. Du Prez, F. E.; Goethals, E. J.; Schué, R.; Qariouh, H.; Schué, F. Segmented Network Structures for the Separation of Water/Ethanol Mixtures by Pervaporation. *Polym. Int.* **1998**, *46*, 117–125.
44. Shamlou, S.; Kennedy, J. P.; Levy, R. P. Amphiphilic Networks. X. Diffusion of Glucose and Insulin (and Nondiffusion of Albumin) through Amphiphilic Membranes. *J. Biomed. Mater. Res.* **1997**, *35*, 157–163.
45. Podual, K.; Doyle, F. J., III; Peppas, N. A. Preparation and Dynamic Response of Cationic Copolymer Hydrogels Containing Glucose Oxidase. *Polymer* **2000**, *41*, 3975–3983.
46. Vamvakaki, M.; Patrickios, C. S. Polyelectrolytic Amphiphilic Model Networks in Water: A Molecular Thermodynamic Theory for Their Microphase Separation. *J. Phys. Chem. B* **2001**, *105*, 4979–4986.
47. Wu, K.-A.; Jha, P. K.; Olvera de la Cruz, M. Pattern Selection in Polyelectrolyte Gels by Nonlinear Elasticity. *Macromolecules* **2012**, *45*, 6652–6657.
48. Kali, G.; Georgiou, T. K.; Iván, B.; Patrickios, C. S.; Loizou, E.; Thomann, Y.; Tiller, J. C. Synthesis and Characterization of Anionic Amphiphilic Model Co-networks Based on Methacrylic Acid and Methyl Methacrylate: Effects of Composition and Architecture. *Macromolecules* **2007**, *40*, 2192–2200.
49. Longo, G. S.; Olvera de la Cruz, M.; Szleifer, I. Molecular Theory of Weak Polyelectrolyte Gels: The Role of pH and Salt Concentration. *Macromolecules* **2011**, *44*, 147–158.
50. Tagliazucchi, M.; de la Cruz, M. O.; Szleifer, I. Self-Organization of Grafted Polyelectrolyte Layers *via* the Coupling of Chemical Equilibrium and Physical Interactions. *Proc. Natl. Acad. Sci. U.S.A.* **2010**, *107*, 5300–5305.
51. Xu, L.; Iwata, K.; Kobayashi, S.; Ishizone, T.; Satoh, M. Salt Resistivity of Poly(4-Vinyl Benzoic Acid) Gel. *Colloid Polym. Sci.* **2007**, *285*, 485–489.
52. Katchalsky, A.; Spitnik, P. Potentiometric Titrations of Polymethacrylic Acid. *J. Polym. Sci.* **1947**, *2*, 432–446.
53. Katchalsky, A.; Shavit, N.; Eisenberg, H. Dissociation of Weak Polymeric Acids and Bases. *J. Polym. Sci.* **1954**, *13*, 69–84.